Journal of Systems Engineering and Electronics
Vol. 32, No. 2, April 2021, pp.380 – 388

VCR-LFM-BPSK signal design for countering advanced interception technologies

WANG Shanshan, LIU Zheng*, XIE Rong, and WANG Jingjing

National Laboratory of Radar Signal Processing, Xidian University, Xi'an 710071, China

Abstract: The hybrid waveform of linear frequency modulation and binary phase shift keying (LFM-BPSK) can take advantages of the LFM and BPSK signals, and reduce the defects of them. However, with the development of interception technology for the LFM-BPSK signal, the application of the signal is limited. In this paper, to improve the anti-interception performance of the hybrid waveform, a new waveform of LFM-BPSK with the varying chirp rate (denoted as VCR-LFM-BPSK) is designed. In this design, based on the working principle of the interception frame for the LFM-BPSK signal, different chirp rates are introduced in different sub-pulses to prevent the signal from being intercepted by the frame. Then, to further improve the anti-interception performance of the VCR-LFM-BPSK signal, the chirp rates are optimized by minimizing the interception capability of the interceptor. Moreover, based on the VCR-LFM-BPSK signal with the optimized chirp rates, the binary phases are designed via a multi-objective Pareto optimization to improve the capabilities of autocorrelation and spectrum. Simulation results demonstrate that the designed VCR-LFM-BPSK signal outperforms the traditional LFM-BPSK signal in countering the advanced interception technologies.

Keywords: hybrid waveform, waveform design, anti-interception, optimization.

DOI: 10.23919/JSEE.2021.000031

1. Introduction

Electronic intelligence (ELINT) interception is an important part of electronic countermeasures (ECM) which mainly consists of signal detection, signal recognition and signal parameter estimation [1,2]. Based on the intercepted parameters, jamming signals are transmitted by countermeasure systems to weaken the performance of radar. To reduce the probability of interception, researchers propose several methods [3−9], of which the pulse compression signal is an effective one [8,9]. Linear frequency modulation (LFM) and binary phase shift keying (BPSK) are two typical pulse compression signals. The LFM signal can realize large time-bandwidth product conveniently and has a low Doppler sensitivity, but it has a coupling effect of range and velocity. The BPSK signal has a low autocorrelation peak sidelobe level (PSL), but it is sensitive to Doppler frequency shift. In addition to the defects above, both LFM and BPSK signals are prone to be intercepted due to single modulation. Considering this, the hybrid waveform of LFM and BPSK (LFM-BPSK) is proposed to take advantages of the signals and reduce the defects of them [10,11].

However, ECM and electronic counter-countermeasures (ECCM) are developed mutually. To counter the LFM-BPSK signal, the parameter interception technologies for the LFM-BPSK waveform are proposed [12,13]. The main idea is to separate the modulation of the signal, and further to estimate the parameters of LFM and BPSK. The classical parameter interception frame for the LFM-BPSK signal includes three steps, i.e., the square method, chirp rate and frequency estimation, and phase code reconstruction. Based on the interception frame, all parameters of the LFM-BPSK signal can be easily estimated, which adversely affects the signal application in ECM environment.

In this paper, to improve the anti-interception performance of the LFM-BPSK signal, a novel waveform, named as LFM-BPSK with varying chirp rate (VCR-LFM-BPSK), is designed to counter the advanced interception technologies. The contribution of our work is threefold. First, the VCR-LFM-BPSK introduces different chirp rates in different subpulses, which can prevent parameters from being estimated by the interception frame for the LFM-BPSK signal. Second, the chirp rates of the VCR-LFM-BPSK are optimized to avoid the commonly used interception technology called the dechirping method. Finally, the phase codes of the VCR-LFM-BPSK signal are de-

Manuscript received July 05, 2020.
*Corresponding author.
This work was supported by the Equipment Pre-research Field Foundation of China (61404150102) and the National Postdoctoral Program for Innovative Talents (BX20180240).

signed by a multi-objective Pareto optimization, which can improve the autocorrelation and spectrum capabilities of the transmit signal. In numerical examples, the effectiveness of the designed chirp rates and phase codes is verified by comparing with the random sequences. Besides, the performance of the designed VCR-LFM-BPSK signal for countering advanced interception technologies is demonstrated by comparing with traditional radar signals.

The rest of the paper is organized as follows. The VCR-LFM-BPSK signal is developed in Section 2. In Section 3, the parameters of the VCR-LFM-BPSK signal are optimized. Numerical examples are given in Section 4 to demonstrate the effectiveness of the work. Finally, the conclusions are presented in Section 5.

2. LFM-BPSK with VCR

In this section, the VCR-LFM-BPSK signal is developed to prevent transmit parameters from being estimated by the interception frame for the hybrid signal.

As we know, the expression of the LFM-BPSK signal is

$$s(t)=\sum_{i=0}^{I-1}\mathrm{rect}\left(\frac{t-iT_c}{T_c}\right)\mathrm{e}^{\mathrm{j}\pi\left[2f_0(t-iT_c)+K(t-iT_c)^2\right]+\mathrm{j}\phi_i} \tag{1}$$

where I is the number of subpulses, $\mathrm{rect}(t/T_c)$ is a rectangular wave with width T_c, f_0 is the carrier frequency, $\phi_i=\pi\times\{0,1\}$ denotes the binary phase of the $(i+1)$th subpulse, and K is the chirp rate of the signal.

Some interception technologies have been proposed to estimate the parameters of the LFM-BPSK signal [12,13]. The main idea of the multi-parameter estimation for the LFM-BPSK is to separate the modulation of the signal and further to estimate the parameters of the LFM signal and the BPSK signal. Generally, the parameter interception frame for the LFM-BPSK signal consists of three steps in Fig. 1.

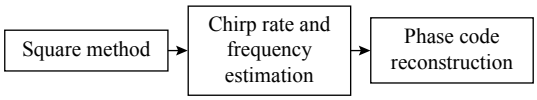

Fig. 1 Parameter interception frame for the LFM-BPSK signal

Performing the square method on the LFM-BPSK signal results in

$$y_1(t)=\left[\sum_{i=0}^{I-1}\mathrm{rect}\left(\frac{t-iT_c}{T_c}\right)\mathrm{e}^{\mathrm{j}\pi\left[2f_0(t-iT_c)+K(t-iT_c)^2\right]+\mathrm{j}\phi_i}\right]^2=$$

$$\sum_{i=0}^{I-1}\mathrm{rect}\left(\frac{t-iT_c}{T_c}\right)\mathrm{e}^{\mathrm{j}2\pi\left[2f_0(t-iT_c)+K(t-iT_c)^2\right]}. \tag{2}$$

It can be seen in (2) that the phase code symbol ±1 of the LFM-BPSK signal is changed to 1 by the square method. Consequently, the parameters of $y_1(t)$ can be estimated by the interception method in [14]. Based on the estimated chirp rate K' and frequency f_0', the reconstructed result of the LFM in (1) is

$$y_{\mathrm{LFM}}=\sum_{i=0}^{I-1}\mathrm{rect}\left(\frac{t-iT_c}{T_c}\right)\mathrm{e}^{\frac{\mathrm{j}\pi}{2}\left[2f_0'(t-iT_c)+K'(t-iT_c)^2\right]}. \tag{3}$$

Then, the baseband BPSK signal can be obtained by multiplying the intercepted LFM-BPSK signal and the conjugate of the LFM signal in (3), which is given as follows:

$$s_{\mathrm{BPSK}}(t)=\sum_{i=0}^{I-1}\mathrm{rect}\left(\frac{t-iT_c}{T_c}\right)\mathrm{e}^{\mathrm{j}\phi_i}. \tag{4}$$

Based on (4), the phase codes can be reconstructed easily.

From the analysis above, since the chirp rates of the LFM-BPSK signal are the same in different sub-pulses, the signal is prone to be intercepted after performing the square method. Accordingly, we introduce different chirp rates in different sub-pulses to form a new waveform named as VCR-LFM-BPSK to improve the anti-interception performance. The expression of the VCR-LFM-BPSK signal can be written as

$$s(t)=\sum_{i=0}^{I-1}\mathrm{rect}\left(\frac{t-iT_c}{T_c}\right)\mathrm{e}^{\mathrm{j}\pi\left[2f_0(t-iT_c)+k_i(t-iT_c)^2\right]+\mathrm{j}\phi_i} \tag{5}$$

where k_i denotes the chirp rate of the $(i+1)$th sub-pulse and satisfies $k_i\neq k_j$, $i\neq j$.

Similarly, performing the square method on the VCR-LFM-BPSK, the output signal is

$$y_2(t)=\left[\sum_{i=0}^{I-1}\mathrm{rect}\left(\frac{t-iT_c}{T_c}\right)\mathrm{e}^{\mathrm{j}\pi\left[2f_0(t-iT_c)+k_i(t-iT_c)^2\right]+\mathrm{j}\phi_i}\right]^2=$$

$$\sum_{i=0}^{I-1}\mathrm{rect}\left(\frac{t-iT_c}{T_c}\right)\mathrm{e}^{\mathrm{j}2\pi\left[2f_0(t-iT_c)+k_i(t-iT_c)^2\right]}. \tag{6}$$

As shown in (6), the output signal for the VCR-LFM-BPSK is composed of multiple LFM signals with different chirp rates, which makes it harder to be estimated by using the method in [14].

From the analysis above, the VCR-LFM-BPSK signal outperforms the traditional LFM-BPSK signal in countering the interception frame in Fig. 1. However, the value of k_i cannot vary without any limits.

On one hand, the maximum value of k_i influences the time resolution. Based on (5), the frequency ranges of the subpulses are shown in Fig. 2.

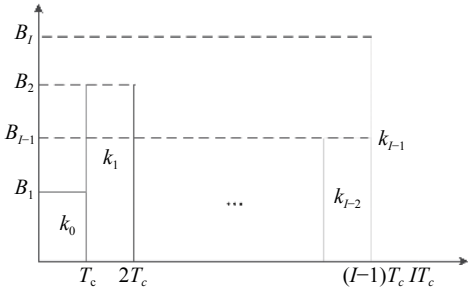

Fig. 2 Frequency ranges of the sub-pulses for the VCR-LFM-BPSK signal

Based on Fig. 2, the time resolution of $s(t)$ can be calculated by $\Delta\tau=\dfrac{1}{k_{\max}T_c}$, where $k_{\max}$ denotes the maximum value of k_i. Thus, the value of $k_{\max}$ should satisfy $\dfrac{1}{T_c\Delta\tau_r}\leqslant k_{\max}\leqslant\dfrac{B_{\text{allow}}}{T_c}$, where $\Delta\tau_r$ is the resolution requirement, and B_{allow} is the maximum bandwidth allowed.

On the other hand, a small value of k_i results in the increase of the spectral peak. The spectrums of the sub-pulses and the VCR-LFM-BPSK signal are shown in Fig. 3 (a) and Fig. 3 (b), respectively.

In Fig. 3, the width of the sub-pulse is 0.1 ms, the phase codes are random variables, and the values of k_i are set as 2 GHz/s, 4 GHz/s, 6 GHz/s, 8 GHz/s and 10 GHz/s, respectively.

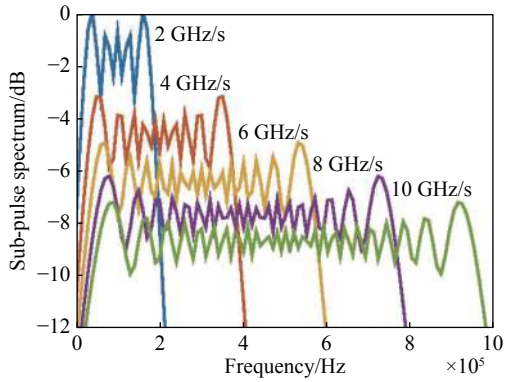

(a) Sub-pulse spectrum

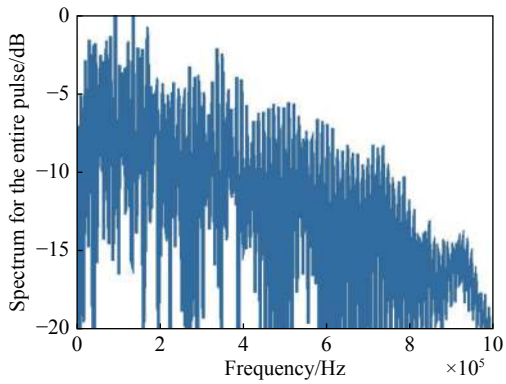

(b) Spectrum of the VCR-LFM-BPSK signal

Fig. 3 Spectrum of VCR-LFM-BPSK signal with five sub-pulses

As shown, the smaller the value of k_i, the larger the peak value of the sub-pulse spectrum, leading to a higher peak in Fig. 3 (b). Since uneven spectrum distribution is not conducive to signal processing, e.g., the weighting method to suppress sidelobes, a too small minimum chirp rate $k_{\min}$ is not suitable.

Based on the analysis above, the values of $k_{\min}$ and $k_{\max}$ can be preset by balancing radar performance. With the presetting range $[k_{\min}, k_{\max}]$, the specific value of k_i will be designed in the following part.

3. Optimization of the parameters

3.1 Optimization of the chirp rates

The dechirping method can effectively decrease the low probability of interception (LPI) performance of the LFM signal by converting the wideband signal into the narrowband signal, so it has been widely used in interceptors. Furthermore, the dechirping method can act on other signals that possess LFM features, like LFM-BPSK and VCR-LFM-BPSK signals. Considering the dechirping signal $\boldsymbol{g}=\mathrm{e}^{\mathrm{j}\pi\nu t^2}$, the output signal after dechirping in the frequency domain is

$$\boldsymbol{y}_{\text{out}}=F\{\widetilde{\boldsymbol{s}}\circ\boldsymbol{g}^*\} \tag{7}$$

where $F\{\cdot\}$ denotes the operator of Fourier transform, $\circ$ denotes the Hadamard product, and $\widetilde{\boldsymbol{s}}$ is the signal sensed by the interceptor. $(\cdot)^*$ denotes the conjugate. Interception mainly consists of signal detection, signal recognition and signal parameter estimation [1,2], of which signal detection is the basis. As is well known from standard detection theory results, the larger the signal-to-noise ratio, the better the detection performance. Therefore, the signal with a lower output peak value (lower signal-to-noise ratio (SNR)) is harder to be detected, i.e., it has a better anti-interception performance. When $\widetilde{\boldsymbol{s}}$ is an LFM waveform, and the chirp rate of $\boldsymbol{g}$ is equal to that of $\widetilde{\boldsymbol{s}}$, a well-defined peak will appear in $\boldsymbol{y}_{\text{out}}$. This suggests that the anti-interception performance of the LFM signal is successfully deteriorated. Obviously, the output peak values for LFM-BPSK and VCR-LFM-BPSK signals are smaller than that for LFM signals. Nevertheless, for a better anti-interception performance, the output peak for the hybrid signal needs to be further decreased.

The output peak μ obtained by dechirping is

$$\mu=\max\{|\boldsymbol{y}_{\text{out}}|\} \tag{8}$$

where $|\cdot|$ denotes the absolute value, max $\{\cdot\}$ denotes the maximum value.

Accordingly, the optimization of chirp rates for countering the dechirping method can be formulated by

$$\min_{\boldsymbol{k}} \mu(\boldsymbol{k})$$
$$\text{s.t. } k_{\min} \leqslant k_i \leqslant k_{\max} \tag{9}$$

where $k_{\min}$ and $k_{\max}$ have been preset based on the analysis in Section 2. In practice, the values that k_i can take are limited and discrete, so the problem formulated in (9) can be solved by the genetic algorithm (GA).

3.2 Optimization of the phase codes

In this subsection, based on the VCR-LFM-BPSK with chirp rates obtained by (9), the phase codes are designed by a Pareto-optimization.

Following the analysis in Section 2, to improve the spectrum ability of the VCR-LFM-BPSK, the phase codes can be optimized as follows:

$$\min_{\boldsymbol{\phi}} \max\{F\{s(\boldsymbol{\phi})\}\}$$
$$\text{s.t. } \boldsymbol{\phi} \in \boldsymbol{\Omega}_2 \tag{10}$$

where $\boldsymbol{\Omega}_2$ represents the finite alphabet codes. Precisely, $\boldsymbol{\Omega}_2 = \{\boldsymbol{c} | c_i \in \psi_2, i = 1, \cdots, I\}$ where $\boldsymbol{c}$ denotes the possible phase code vector and $\psi_2 = \{0, \pi\}$.

Besides, for pulse compression operated at the radar receiver, low autocorrelation PSL is needed to avoid the omission of weak targets. The autocorrelation function of the signal is defined as

$$\boldsymbol{A}_u(\boldsymbol{\phi}) = \int_{-\infty}^{\infty} s(\tau, \boldsymbol{\phi}) s^*(\tau - t, \boldsymbol{\phi}) \mathrm{d}\tau. \tag{11}$$

Following (11), the PSL of the autocorrelation function can be written as

$$PSL(\boldsymbol{\phi}) = \max\{\boldsymbol{W} | \boldsymbol{A}_u(\boldsymbol{\phi})|\} \tag{12}$$

where $\boldsymbol{A}_u$ denotes the discrete form of the autocorrelation function, and $\boldsymbol{W}$ is defined as

$$\boldsymbol{W} = \mathrm{diag}[1, \cdots, 1, 0, \cdots, 0, 1, \cdots, 1] \tag{13}$$

where $\mathrm{diag}[\cdot]$ is a diagonal matrix with diagonal elements given by the vector in the brackets. Based on the relationship of $\Delta\tau = \dfrac{1}{k_{\max} T_c}$, the number of 0 in (13) is equal to the value of $\dfrac{f_s}{k_{\max} T_c}$, where f_s is the sampling frequency.

Then, by simultaneously considering the autocorrelation and spectrum as performance guideline, the phase code optimization problem can be formulated as follows:

$$\min_{\boldsymbol{\phi}} \max\{F\{s(\boldsymbol{\phi})\}\}, \quad PSL(\boldsymbol{\phi})$$
$$\text{s.t. } \boldsymbol{\phi} \in \boldsymbol{\Omega}_2. \tag{14}$$

Model (14) is a multi-objective optimization problem (MOP) which usually cannot generate a feasible solution that satisfies all the objectives [15−17], so it is a typical Pareto-optimization. The feasible method to obtain the Pareto-optimal solution is the weighted sum, i.e.,

$$\min_{\boldsymbol{\phi}} w \cdot \max\{F\{s(\boldsymbol{\phi})\}\} + (1 - w)(PSL(\boldsymbol{\phi}))$$
$$\text{s.t. } \boldsymbol{\phi} \in \boldsymbol{\Omega}_2 \tag{15}$$

where the weighting $0 \leqslant w \leqslant 1$ is used to adjust the contribution of the spectrum to the objective function. Obviously, the problem in (15) can be also solved by the genetic algorithm (GA).

Finally, by substituting the optimized $\boldsymbol{k}'$ and $\boldsymbol{\phi}'$ into (5), the VCR-LFM-BPSK signal is obtained.

4. Numerical examples

In this section, some numerical examples are presented to demonstrate the effectiveness of our work. For the VCR-LFM-BPSK signals in the following examples, the number of sub-pulses $I = 15$, and the sub-pulse width $T_c = 10$ μs. Balancing radar performance, the chirp rate range $[k_{\min}, k_{\max}]$=[80 GHz/s, 100 GHz/s] unless otherwise stated. Correspondingly, the time-bandwidth product of the signal is approximately equal to 150. Simulations are divided into three parts. In the first part, the effectiveness of the modeled optimization for designing signal parameters is verified. In the second part, simulations are presented to analyze the ambiguity function of the designed signal. In the third part, we demonstrate the anti-interception superiority of the designed signal.

4.1 Analysis of the optimized signal parameters

In this subsection, the effectiveness of the modeled optimizations is verified by comparing the optimized parameters with the random sequences.

At first, after performing the dechirping method, the output signals for the optimized and random chirp rates are given in Fig. 4. As shown, the peak value for the optimized chirp rates is 5.18 dB less than that for the random chirp rates, which demonstrates the effectiveness of the optimization in (9).

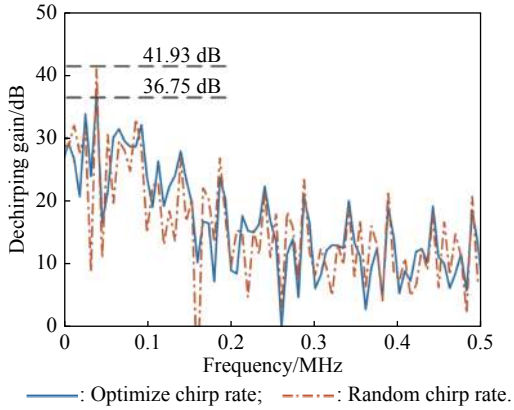

Fig. 4 Output signals after dechirping

Based on the VCR-LFM-BPSK with optimized chirp rates, the phase codes can be obtained by the optimization in (15). The formulation in (15) is a performance

tradeoff problem, i.e., the higher the value of w, the higher the autocorrelation PSL and the lower the spectral peak. Specially, with $w = 1$, only the spectrum ability is optimized. In this case, the spectrums obtained by optimized and random codes are presented in Fig. 5. As shown, the spectral peak value for the optimized phase codes is 5.22 dB less than that for the random codes, which verifies the effectiveness of the optimization in suppressing the spectral peak.

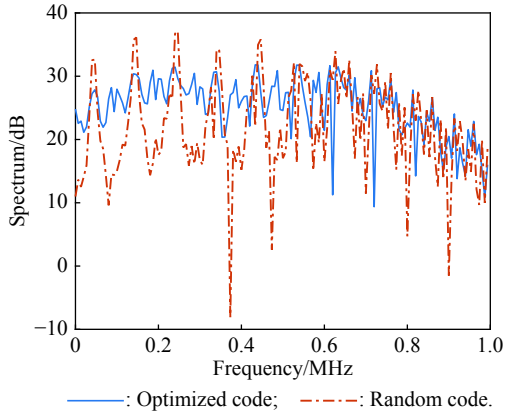

Fig. 5 Spectrums of the optimized and random phase codes

Similarly, with $w = 0$, only the autocorrelation ability is optimized. The autocorrelation functions determined by the optimized and random codes are presented in Fig. 6. The PSL of the autocorrelation for the optimized and random phase codes are equal to −18.61 dB and −8.435 dB, respectively. These outcomes certify the feasibility of the optimization in suppressing autocorrelation sidelobes.

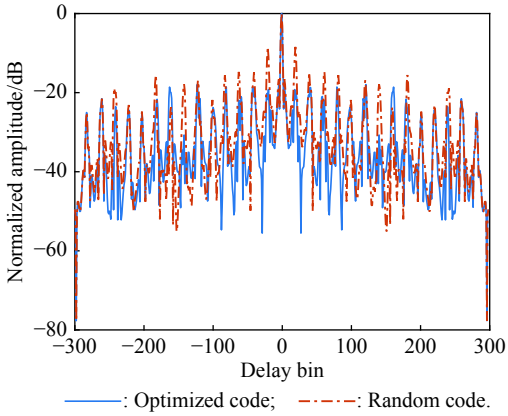

Fig. 6 Autocorrelation functions of the optimized and random phase codes

The Pareto curve is given in Fig. 7. With w varying from 0 to 1, the spectral peak is from 33 dB to 31.9 dB, and autocorrelation PSL is from −18.61 dB to −13.75 dB. As expected, w trades off the performance of the autocorrelation and spectrum, which is the classical feature of the bi-objective Pareto curve, i.e., any solution can be a Pareto-optimized point.

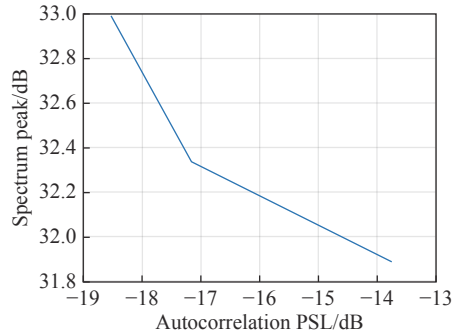

Fig. 7 Pareto-optimized curve

4.2 Analysis of the VCR-LFM-BPSK signal from a radar point of view

Since the ambiguity function is an effective tool for analyzing waveform performance, the ambiguity function of the VCR-LFM-PC signal is analyzed in this subsection.

The definition of the baseband LFM-BPSK signal can be rewritten as $s(t) = v(t) * u(t)$, where $v(t) = \mathrm{rect}(t/T_c)\mathrm{e}^{\mathrm{j}\pi Kt^2}$, $u(t) = \sum_{i=0}^{I-1} \mathrm{e}^{\mathrm{j}\phi_i}\delta(t - iT_c)$, and $*$ denotes the convolution. Therefore, the ambiguity function of the LFM-BPSK waveform can be obtained by $\chi(\tau, f_d) = \chi_1(\tau, f_d) * \chi_2(\tau, f_d)$ where $\chi_1(\tau, f_d)$ and $\chi_2(\tau, f_d)$ are the ambiguity functions of $v(t)$ and $u(t)$, respectively. Accordingly, the ambiguity function of the LFM-BPSK combines the ambiguity characteristics of the LFM signal and the BPSK signal. The VCR-LFM-BPSK signal is a combination of subpulses from different LFM-BPSK signals with different chirp rates. The smaller the chirp rate, the less LFM feature in the subpulse. Especially, when the chirp rate is 0 GHz/s, the subpulse belongs to BPSK. Therefore, under the same bandwidth, the ambiguity function of the VCR-LFM-BPSK is more thumbtack-typed than that of the LFM-BPSK. Moreover, the smaller the value of the chirp rate, the more thumbtack-typed the ambiguity function of the VCR-LFM-BPSK signal.

Consider the baseline LFM, BPSK and LFM-BPSK waveforms with the same bandwidth B as the VCR-LFM-BPSK. For the LFM signal, the pulse width $T_p = 15T_c = 150$ μs. For the BPSK signal, the sub-pulse width $T_c = 1/B$, the number of the sub-pulses is 150, and the phase codes are generated randomly. For the LFM-BPSK signal, the bandwidth of the sub-pulse is B, and the rest of parameters are consistent with the VCR-LFM-BPSK. The ambiguity figures are given in Fig. 8. As expected, the ambiguity functions are oblique blades and thumbtack typed for LFM and BPSK, respectively. For LFM-BPSK and VCR-LFM-BPSK signals, the ambiguity functions are approximately thumbtack-typed with $(2I-1)$ oblique

blades. Moreover, it can be seen in Fig. 8(c)−Fig. 8(e) that the ambiguity function of the VCR-LFM-BPSK signal becomes closer to thumbtack-typed as the lower bound of chirp rates decreases.

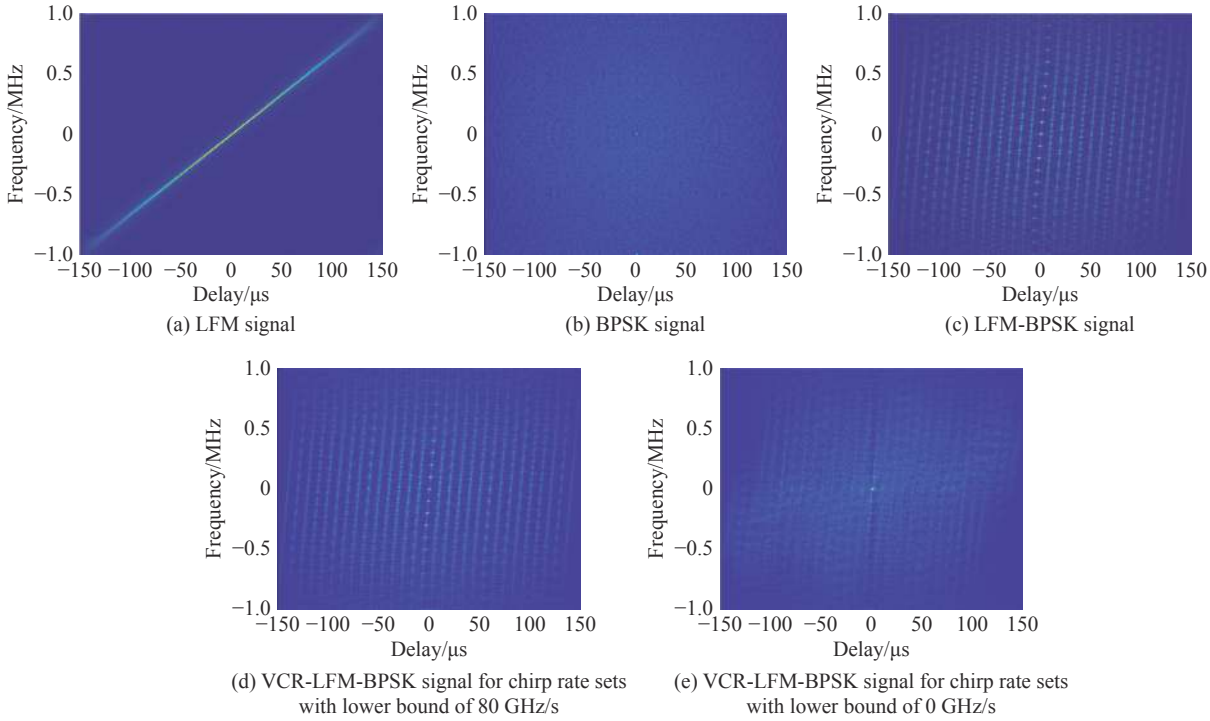

(a) LFM signal (b) BPSK signal (c) LFM-BPSK signal

(d) VCR-LFM-BPSK signal for chirp rate sets with lower bound of 80 GHz/s

(e) VCR-LFM-BPSK signal for chirp rate sets with lower bound of 0 GHz/s

Fig. 8 Ambiguity figures

The pulse compressing results under different Doppler shifts are given in Fig. 9. As shown, the LFM signal has a low Doppler sensitivity but suffers from the coupling effect of range and velocity. The BPSK signal is sensitive to Doppler frequency shift but solves the problem of range-Doppler coupling. In contrast, both LFM-BPSK and VCR-LFM-BPSK signals reduce the effect of range-velocity coupling on the LFM and the effect of Doppler sensitivity on the BPSK. As shown in Fig. 9, the VCR-LFM-BPSK signal has a better sidelobe ability than the LFM-BPSK signal in the case of both $f_d = 0$ MHz and $f_d = 0.1$ MHz. Specifically, when $f_d = 0$ MHz, the output peak ratio of mainlobe to sidelobe (RMS) are 17.94 dB and 9.54 dB for VCR-LFM-BPSK and LFM-BPSK, respectively. When $f_d = 0.1$ MHz, the output RMSs are 13.66 dB and 9.53 dB for VCR-LFM-BPSK and LFM-BPSK, respectively. Although the sidelobes of the VCR-LFM-BPSK are lower than that of the LFM-BPSK when $f_d = 0$ MHz and $f_d = 0.1$ MHz, the loss of the VCR-LFM-BPSK caused by the Doppler frequency is higher. To better illustrate the loss, the normalized pulse compressing results of the VCR-LFM-BPSK, including the mainlobe width (MW) (−3 dB), the RMS and the main lobe gain (MG), are given in Table 1. As shown, compared with the case of $f_d = 0$ MHz, the loss of the MW, RMS and MG for the VCR-LFM-BPSK under $f_d = 0.1$ MHz are 0.96×10^{-7} s, 4.28 dB and 1.51 dB, respectively.

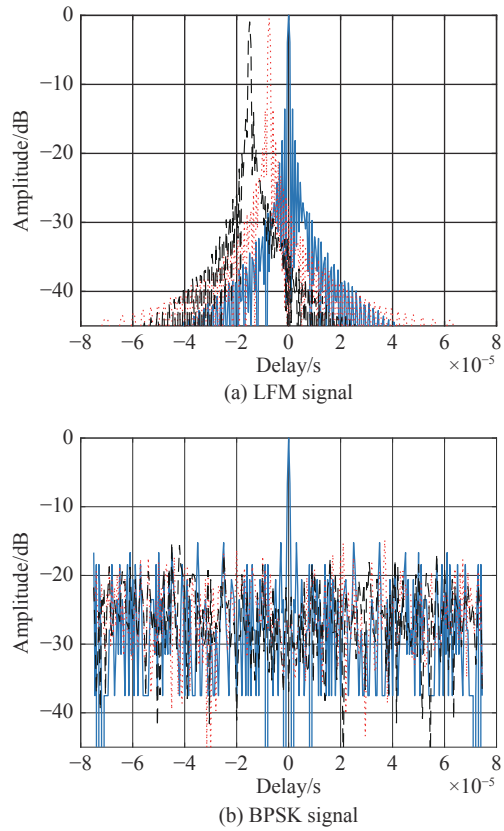

(a) LFM signal

(b) BPSK signal

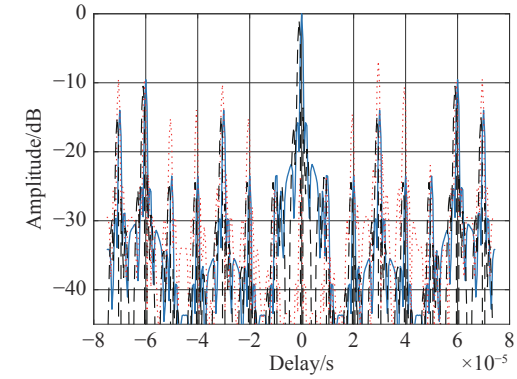

(c) LFM-BPSK signal

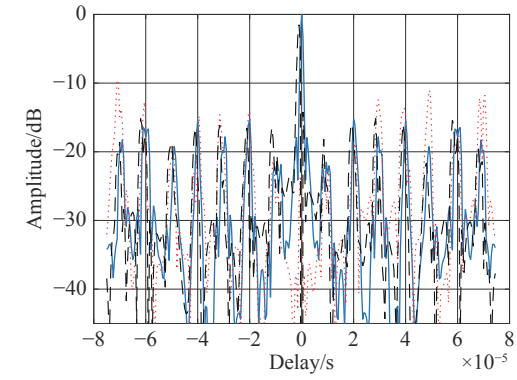

(d) VCR-LFM-BPSK signal

——: f_d=0 MHz; ·····: f_d=0.05 MHz; — — —: f_d=0.1 MHz.

Fig. 9 Pulse compressing results

Table 1 Pulse compressing performance under different Doppler shifts

Doppler shift/MHz	MW/s	RMS/dB	MG/dB
0	9.44×10^{-7}	17.94	0
0.1	1.04×10^{-6}	13.66	−1.51

4.3 Analysis of anti-interception performance

In this subsection, we demonstrate the performance of the designed VCR-LFM-BPSK signal in countering advanced interception technologies.

Case 1 In this case, based on the assumption that the interception frame in Fig. 1 is taken by the interceptor, the anti-interception performance of the VCR-LFM-BPSK signal is assessed by comparing with other radar signals.

The average estimation errors are used as the metrics to assess the ability of the VCR-LFM-BPSK signal in countering the interception frame in Fig. 1. Let $\hat{f}$ denote the carrier frequency estimation. $\hat{k}_i$ and $\hat{\phi}_i$ denote the chirp rate estimation and the phase code estimation for the $(i+1)$th subpulse, respectively. $\sum_{i=0}^{I-1}\left(\phi_i \neq \hat{\phi}_i\right)$ is used to count the number of wrong phase code estimations. The average estimation errors of the carrier frequency, chirp rates and phase codes are denoted by e_f, e_k and e_ϕ, respectively, where $e_f = \mathrm{E}\left[\left|f_0 - \hat{f}\right|\right]$, $e_k = \mathrm{E}\left[\frac{1}{I}\sum_{i=0}^{I-1}\left|k_i - \hat{k}_i\right|\right]$, and $e_\phi = \mathrm{E}\left[\sum_{i=0}^{I-1}\left(\phi_i \neq \hat{\phi}_i\right)\right]$. $\mathrm{E}[\cdot]$ denotes the operator of taking expectation. The method of discrete polynomial transform (DPT) in [14] is introduced to estimate the signal parameters after performing the square method.

With 500 Monte Carlo experiments, Fig. 10 shows the average estimation errors for LFM-BPSK and VCR-LFM-BPSK signals with SNR varying from 1 dB to 10 dB. As observed, the estimation error decreases with the increase of SNR, and under the same SNR, the estimation errors for the LFM-BPSK signal are lower than that for the VCR-LFM-BPSK signal. Precisely, when SNR is 4 dB, the estimation errors of the frequency and the chirp rate for the VCR-LFM-BPSK signal are 74 Hz and 37 kHz/s, respectively. In contrast, for the LFM-BPSK signal, the estimation errors of the frequency and the chirp rate are 11 Hz and 4 kHz/s, respectively. Besides, the chirp rate estimation results for the VCR-LFM-BPSK signal are far from the real values even when the curve converges to the stable state. Substituting the chirp rate and frequency estimation results in (3), the phase codes can be reconstructed by multiplying the intercepted signal and the conjugate of the signal in (3). The phase code reconstruction errors with different SNRs are shown in Fig. 10 (c). As shown, when SNR is 4 dB, the average estimation error for the LFM-BPSK signal is close to 0 while the average error for the VCR-LFM-BPSK signal is greater than 2.

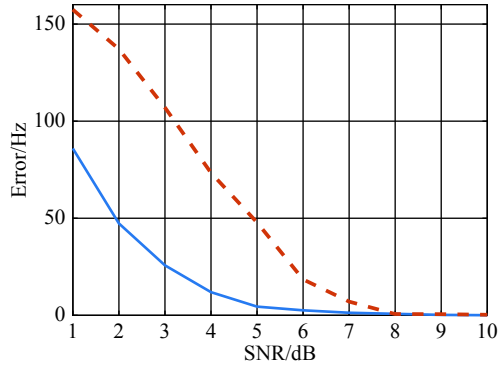

——: LFM-BPSK; — — —: VCR-LFM-BPSK.

(a) Frequency estimation errors

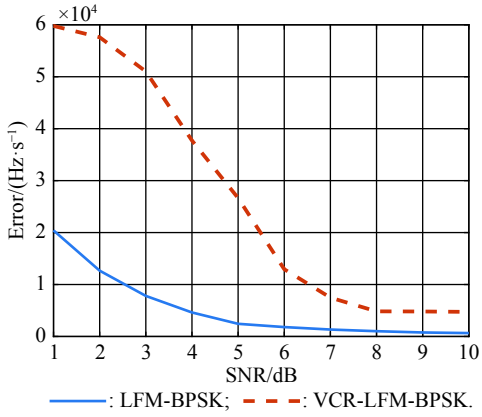

(b) Chirp rate estimation errors

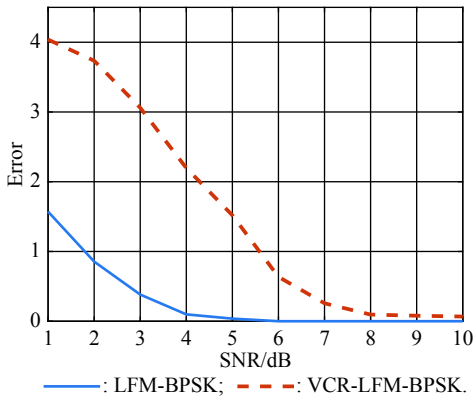

(c) Phase code estimation errors

Fig. 10 Parameter estimation results for the LFM-BPSK and VCR-LFM-BPSK signals with different SNRs

Assuming that the sensed signal can be recognized before being estimated, only the last two steps in the interception frame are used to estimate the parameters of the LFM and BPSK signals. The estimation errors are given in Fig. 11 and Fig. 12. Obviously, compared with the LFM-BPSK and VCR-LFM-BPSK, the ani-interception performance of the LFM and BPSK signals is poor.

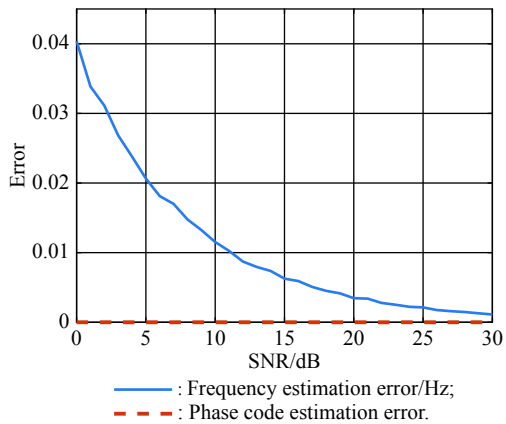

Fig. 11 Estimation errors for the BPSK signal

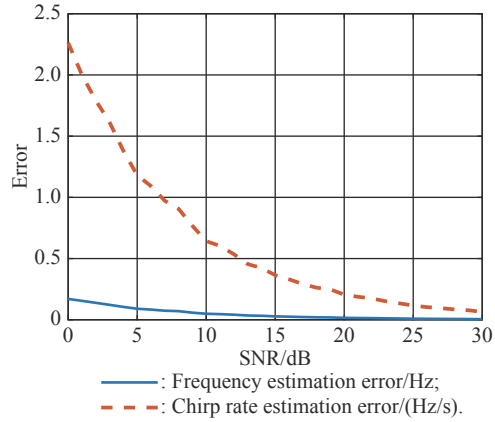

Fig. 12 Estimation errors for the LFM signal

All the outcomes above highlight that the VCR-LFM-BPSK signal outperforms the traditional radar signals when countering the interception frame in Fig. 1.

Case 2 Traditional interceptors cannot intercept signals which are submerged in the noise. Since the dechirping method can effectively improve the spectral peak of the signal, it has been widely used in interceptors. In this case, we analyze the ability of the VCR-LFM-BPSK signal in countering the dechirping method.

Assuming that the value of v for the dechirping signal $e^{j\pi vt^2}$ sweeps from 0 GHz/s to 100 GHz/s, the dechirping results are given in Fig. 13. We can see that the BPSK signal has the best ability of anti-dechirping due to the fewer LFM features. Nevertheless, considering that the BPSK signal can be easily intercepted based on the phase code reconstruction methods, it cannot adapt well to modern ECM environment. Besides, the dechirping gains for the VCR-LFM-BPSK, LFM-BPSK, and LFM signals are 36.75 dB, 41.74 dB, and 49.54 dB, respectively. Obviously, the performance of the VCR-LFM-BPSK signal in countering the dechirping method is superior.

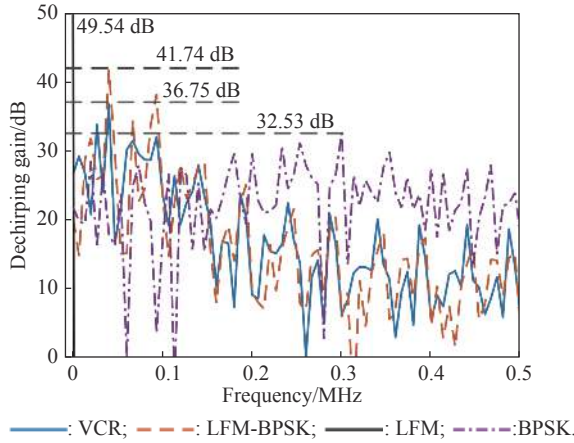

Fig. 13 Results of dechirping

5. Conclusions

In this paper, to improve the anti-interception performance of the hybrid waveform, the VCR-LFM-BPSK signal is designed, including the design of signal modulation and that of optimizing signal parameters. Simulation results demonstrate that the designed VCR-LFM-BPSK signal outperforms the traditional radar signals in countering advanced interception technologies. The important contribution of this paper is that a new idea of anti-interception waveform design is proposed, i.e., designing the waveform by countering specific interception technologies and minimizing the performance of hostile interceptors. Compared with the traditional LPI waveform design based on the definition of the intercept factor, the proposed idea is more adaptable to the modern interception environment where advanced interception technologies are continuously developed.

References

[1] LI N J, ZHANG Y T. A survey of radar ECM and ECCM. IEEE Trans. on Aerospace and Electronic Systems, 1995, 31(3): 1110–1120.
[2] GOVONI M A, LI H B, KOSINSKI J A. Low probability of interception of an advanced noise radar waveform with linear-FM. IEEE Trans. on Aerospace and Electronic Systems, 2013, 49(2): 1351–1356.
[3] AVITZOUR D. SNR/bandwidth tradeoff in coherent radar sampling. IEEE Trans. on Aerospace and Electronic Systems, 1990, 26(2): 403–405.
[4] GARDNER W. Spectral correlation of modulated signals: part I-analog modulation. IEEE Trans. on Communications, 1987, 35(6): 584–594.
[5] ZHANG Z K, ZHU J H, TIAN Y B, et al. Novel sensor selection strategy for LPI based on an improved IMMPF tracking method. Journal of Systems Engineering and Electronics, 2014, 25(6): 1004–1010.
[6] BELL M R. Information theory and radar waveform design. IEEE Trans. on Information Theory, 1993, 39(5): 1578–1597.
[7] RAVIER P, AMBLARD P O. Combining an adapted wavelet analysis with fourth-order statistics for transient detection. Signal Processing, 1998, 70(2): 115–128.
[8] SCHLEHER D C. Low probability of intercept radar. Proc. of the International Radar Conference, 1985: 346−349.
[9] WILEY R. ELINT: the interception and analysis of radar signals. Boston: Artech House, 2006.
[10] SHI S Z, ZHAO Z Y, LIU J N. Comparison of radar waveforms combining pseudo-random binary phase coding and chirp modulation for a high-frequency monostatic radar. IET Radar, Sonar, and Navigation, 2016, 10(5): 935–944.
[11] SONG X F, ZHOU S L, WILLETT P. Reducing the waveform cross correlation of MIMO radar with space-time coding. IEEE Trans. on Signal Processing, 2010, 58(8): 4213–4224.
[12] QIU Z Y, ZHU J, LI F. Multiple BPSK/LFM hybrid modulated signals parameter estimation and analysis intercepted by non-cooperative radar receiver. Proc. of the IEEE International Conference on Computational Electromagnetics, 2018: 1−4.
[13] HE D N, ZHANG T Q, GAO L G, et al. Blind estimation for PN code of LFM-PRBC signal based on DPT and spectrum shifting. Proc. of the International Congress on Image and Signal Processing, 2012: 1430−1434.
[14] PELEG S, PORAT B. Linear FM signal parameter estimation from discrete-time observations. IEEE Trans. on Aerospace and Electronic Systems, 1991, 27(4): 607–616.
[15] KERAHROODI M A, AUBRY A, MAIO A D, et al. Coordinate-descent framework to design low PSL/ISL sequences. IEEE Trans. on Signal Processing, 2017, 65(22): 5942–5956.
[16] WU G F, WAN K F, GAO X G, et al. Placement of unmanned aerial vehicles as communication relays in two-tiered multi-agent system: clustering based methods. Journal of Systems Engineering and Electronics, 2020, 31(2): 231–242.
[17] SRINIVAS N, DEB K. Multi-objective optimization using nondominated sorting in genetic algorithms. Evolutionary Computation, 1994, 2(3): 221–248.

Biographies

WANG Shanshan was born in 1996. She received her B.S. degree in communication engineering from Qufu University, Qufu, China, in 2017. She is currently working toward her Ph.D. degree in the National Laboratory of Radar Signal Processing, Xidian University, Xi'an. Her major research interest is multiple-input multiple-output (MIMO) radar signal processing with emphasis on waveform designing.
E-mail: 18392138259@163.com

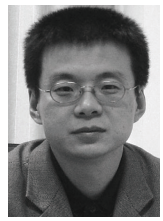

LIU Zheng was born in 1964. He received his B.S., M.S., and Ph.D. degrees in 1985, 1991, and 2000, respectively. He is currently a professor, a doctoral director, and the vice director of the National Laboratory of Radar Signal Processing with Xidian University, Xi'an, China. His research interests include the theory and system design of radar signal processing, precision guiding technology, and multi-sensor data fusion.
E-mail: lz@xidian.edu.cn

XIE Rong was born in 1982. He received his B.S., M.S. and Ph.D. degrees from Xidian University, Xi'an, China, in 2003, 2006, and 2011, respectively. He is currently an associate professor at the National Laboratory of Radar Signal Processing, Xidian University. His major research interests are multiple-input multiple-output (MIMO) radar signal processing, target motion parameter estimation, and real-time implementation.
E-mail: rxie@mail.xidian.edu.cn

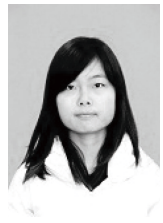

WANG Jingjing was born in 1993. She received her B.S. degree in information countermeasure technology from Xidian University, Xi'an, China, in 2015. She is currently pursuing her Ph.D. degree in signal processing at the National Laboratory of Radar Signal Processing. Her research interests include radar high resolution range profile (HRRP) target recognition and polarization information processing.
E-mail: wangjj0523@163.com